Journal of Materials Chemistry B

Accepted Manuscript

ROYAL SOCIETY OF CHEMISTRY

www.rsc.org/materialsB

Journal of Materials Chemistry B RSCPublishing

ARTICLE

Ultra-high relaxivity iron oxide nanoparticles confined in polymer nanospheres for tumor MR imaging

Cite this: DOI: 10.1039/xoxxoooooox

Received ooth January 2012,
Accepted ooth January 2012

DOI: 10.1039/xoxxoooooox

www.rsc.org/Materials B

Ying Lin,[a] Sanxi Wang,[b] Yajun Zhang,[b] Jiangang Gao,[a] Liu Hong, [a] Xin Wang,[b] Wei Wu,[b] Xiqun Jiang*[b]

Superparamagnetic iron oxide nanoparticles encapsulated in hydrophilic chitosan nanospheres were prepared by nonsolvent-aided counterion complexation in complete aqueous solution. The T_2 relaxation of these hybrid nanospheres in vitro and in vivo was investigated. It is found that the molar transverse relaxivity rate r_2 of hybrid nanospheres is highly dependent on the payload of iron oxide nanoparticles within hybrid nanospheres. Compared to free iron oxide nanoparticles, the molar transverse relaxivity rate r_2 of hybrid nanospheres shows an approximately 8-fold increase and reaches the maximum of 533 Fe mM^{-1} s^{-1}. Such high r_2 value is probably associated with the clustering effect of iron oxide nanoparticles which are confined in the chitosan nanospheres. The in vivo magnetic resonance imaging (MRI) demonstrates that the hybrid nanospheres shorten transverse relaxation time T_2 and significantly decrease signal intensity of tumor area, giving rise to a high contrast tumor MR imaging at a relatively low dose.

Introduction

Magnetic resonance imaging (MRI) is a powerful diagnostic tool in providing noninvasive and real-time detection of diseases or deficiencies such as tumorigenesis and injuries in the liver, spleen and bone marrow.[1,2] However, cellular and molecular imaging in MRI suffers low sensitivity and specificity. As a result, the use of effective contrast agents to enhance diagnostic sensitivity and specificity has been actively pursued. Superparamagnetic iron oxide nanoparticles (SPIO NPs) are served as excellent negative contrast agents, which shorten transverse relaxation time T_2 of protons by the inhomogeneous magnetic field around the nanoparticles, resulting in a darkening effect to improve contrast in T_2-weighted MR imaging.[3] Currently, the most challenges of SPIO NPs are the dose-dependent toxicity, targeting imaging with high sensitivity, fast clearance and unfavorable imaging in organs and tissues outside macrophage-rich organs (liver and spleen).[4] To address these issues, tremendous effort has been devoted and several strategies have been proposed.[5-21] An important approach is to increase the relaxivity of the magnetic particles to enhance the contrast effect. To this end, various iron oxide nanoparticles possessing high relaxation rates have been synthesized, such as Mn- or Zn-doped particles.[22-24] But risk of metal leakage limits their applications in *in vivo* imaging. Alternatively, it has been reported that a hydrophilic polymer coating can increase the transverse relaxivity (r_2) by enhancing the interaction between the water protons and the magnetic fields near the SPIO NPs.[25-27] Multiple SPIO NPs can be assembled into densely packed clusters within polymer matrix driven by special interactions, such as hydrogen bonding or hydrophobic interaction etc. Wrapping the clustered magnetic nanoparticles in the interior of polymer can greatly shorten the intra-particle distance, which decreases with the increase of the nanoparticle loading in polymeric micelles.[28] Also, it has been pointed out that shortening the distance between the clustered magnetic nanoparticles inside polymer micelles may lead to a synergistic increase in T_2 relaxivity.[12,28] Moreover, Weissleder et al. has found that the nanoassembly of SPIO NPs can reduce their magnetic spin-spin relaxation times in water.[29] Since then, a larger number of experimental and theoretical works have demonstrated that the clusters of superparamagnetic nanoparticles enhance r_2 relaxivity rate.[12,28,30-32] As a result, more attention has been paid to enwrapping magnetic nanoparticles with polymer micelles to increase the T_2 relaxation rate of the nanoparticles.[17,25-28,33-37] In addition, encapsulation of magnetic particles with polymer micelles can prolong the circulation time of magnetic nanoparticles and achieve efficient tumor accumulation for *in vivo* tumor imaging.[6,38] Therefore, preparation of clustering SPIO nanoparticles-encapsulated hybrid polymer nanospheres with controllable size and high relaxivity is great important for oncology diagnosis.

Chitosan (CS) is a linear natural polysaccharide composed of N-acetylglucosamine and glucosamine units, and prepared from N-deacetylation of chitin extracted from crustacean shells. Because of its good biocompatible and biodegradable, chitosan has been widely used in biomedical field as the carrier for drug or other functional materials.[39-41] Compared with other biological polymers, chitosan is a cationic polyelectrolyte which will enhance the cellular binding and internalization of the enwrapped materials. Also, it has muco-

adhesive property that prolongs its retention to targeted substrates.[42] The abundant functional groups in chitosan will endow the materials with flexibility in the design of surface chemistry when chitosan is chosen as an envelope material.

In this work, we focus on the enhancement of the r_2 relaxivity and tumor detection sensitivity of hydrophilic superparamagnetic Fe_3O_4 nanoparticles in MRI by enwrapping Fe_3O_4 nanoparticles with biocompatible and hydrophilic CS. By doing so, the Fe_3O_4 nanoparticles would be in a hydrophilic environment, which would enhance significantly the interaction between the nanoparticles and water, and the crosslinked CS outer layer would enhance the stability of the hybrid system in aqueous media thanks to its abundant hydrophilic groups. We prepared size-controllable CS-SPIO hybrid nanospheres in complete aqueous solution without the aid of surfactant and emulsion phase. By virtue of clustered Fe_3O_4 nanoparticles inside the CS matrix, a reproducible platform is provided to tune relaxation rate of the obtained contrast agents. We demonstrate that the resultant hybrid nanospheres are not only stable in aqueous solution, but also have a very high molar transverse relaxivity rate r_2 (up to 533.3 Fe mM^{-1} s^{-1}). Moreover, in vivo imaging in tumor-bearing mice indicates that the CS-SPIO hybrid nanospheres can accumulate in tumor tissue efficiently by the enhanced permeability and retention (EPR) effect and thus enhance MRI tumor contrast at a relatively low dose of nanoparticles. Therefore, CS-SPIO hybrid nanospheres have the potential as ultra-sensitive MRI probes for the diagnosis of developing tumors *in vivo*.

Experimental

Materials

Water-soluble chitosan (CS) with an average molecular weight (Mn) of 5 kDa was purchased from Yuhuan Biomedical Company (Zhejiang, China) and used without further purification. Ethylene diamine tetraacetic acid (EDTA), glutaraldehyde (GA), tetraethylene glycol (TEG), iron (III) acetylacetonate ($Fe(acac)_3$) and NIR-797 isothiocyanate were purchased from Sigma-Aldrich. Fluorescein isothiocyanate (FITC) was provided by Shenggong Company (Shanghai, China). All chemicals were used as received. All ingredients were analytical grade unless otherwise stated. Human neuroblastoma SH-SY5Y cell line, human epithelial carcinoma HeLa cell line and murine hepatic H_{22} cell line were obtained from Shanghai Institute of Cell Biology (Shanghai, China). Male ICR mice (6-8 weeks old) were purchased from Animal Center Laboratory of Nanjing Medical University (Nanjing, China).

Preparation of superparamagnetic iron oxide (SPIO) nanoparticles

Water-soluble Fe_3O_4 nanopaticles were prepared according to the procedures reported previously.[17,43] A mixture of $Fe(acac)_3$ (1.059 g, 3 mmol) and TEG (25 mL) was heated to 110 ^oC with vigorous magnetic stirring under a nitrogen atmosphere. After heating for 1 h, the reaction system was continuously heated to 210 ^oC for 2 h, and then refluxed at 295 ^oC for 1 h. After cooling down to room temperature, diethyl ether was added into the reaction system and a black rough product was precipitated and separated via centrifugation (12000 rpm). The precipitate was washed with diethyl ether and ethanol twice. Finally, the superparamagnetic Fe_3O_4 nanoparticles were obtained by drying the precipitate under vacuum.

Preparation of CS-SPIO hybrid nanospheres

50 mg of chitosan and a certain amount of EDTA were dissolved in 8 mL of deionized water under magnetic stirring. Then, 10 mg SPIO nanoparticles dispersed in aqueous solution (2 mL) were subsequently added to the CS-EDTA mixture aqueous solution. The resultant mixture was sonicated for 10 min and stirred for 4 h. After that, ethanol, a nonsolvent for both chitosan and EDTA, was added dropwise to the system under stirring until the clear solution turned opalescent, which indicated the formation of CS-EDTA nanospheres and SPIO nanoparticles were spontaneously encapsulated into CS-EDTA nanospheres. Then, 30 μL of GA solution (25%) was introduced to cross-link the obtained hybrid nanospheres at room temperature for 4 h. The obtained suspension was filtrated and the sediment was redispersed in deionized water. Finally, the nanosphere solution was dialyzed against deionized water for 48 h to remove EDTA component completely in the spheres to obtain CS-SPIO hybrid nanospheres.

Charaterization

Fourier transform infrared (FT-IR) spectra were recorded on a Nicolet iS10FT-IR spectrometer (Thermo, USA). The hydrodynamic diameters and distribution of the hybrid nanospheres were determined by a dynamic light scattering (DLS) method using a Brookhaven BI-9000AT instrument (Brookhaven Instruments Corporation). All results were the average of triplicate measurements. X-ray powder diffraction patterns of the samples were collected on a Shimadzu XRD-6000 Diffractometer using the Cu-Kα radiation. Morphological observations of Fe_3O_4 nanoparticles (NPs) and the hybrid nanospheres were carried out using high-resolution transmission electron microscopy (HRTEM) (JEM-2100, JEOL), TEM (JEM-200CX), scanning electron microscopy (SEM) (S-4800, Hitachi). Thermogravimetry analyses (TGA) were performed using a TAC71DX thermal analyzer under air flow in the temperature range 25-800 ^oC at a heating rate of 10 ^oC min^{-1}. The iron concentrations were quantified using inductively coupled plasma atomic emission spectroscopy (ICP-AES) (J-A1100, Jarrell-Ash). Digestion of the samples was performed in concentrated nitric acid and heated to 100 ^oC for 6 h before measurements. Magnetic measurements were carried out using a superconducting quantum interference device (SQUID) magnetometer (MPMSXL-7, Quantum Design) with a magnetic field up to 7.0 T. MR relaxometry was performed on a 7.0 T Micro-MR scanner (PharmaScan 70/17, Brucker). The instrumental parameters were set as follows: TR/TE = 3000 ms/40 ms, field of view (FOV) = 3.5 × 4.1 cm, matrix size = 256 × 256, and slice thickness = 1 mm.

SPIO nanoparticles loading level

For the measurement of SPIO loading content and encapsulation efficiency, a stock solution of CS-SPIO hybrid nanospheres was centrifuged and the sediment was lyophilized. Freeze-dried hybrid nanospheres were weighted and then analyzed by TGA. The amount of free SPIO NPs in the supernatant was quantified using ICP-AES. The SPIO NPs loading levels were calculated by equations as follows:

$$\text{SPIO NPs encapsulation efficiency (\%)} = \frac{\text{Weight of SPIO NPs in the hybrid nanospheres}}{\text{Weight of the SPIO NPs in the feed}} \times 100\%$$

$$\text{SPIO NPs loading content (\%)} = \frac{\text{Weight of SPIO NPs in the hybrid nanospheres}}{\text{Weight of the hybrid nanospheres}} \times 100\%$$

Cytotoxicity assays

The in vitro cytotoxicity of the hybrid nanospheres was evaluated by standard MTT assays using human neuroblastoma SH-SY5Y cells and human epithelial carcinoma HeLa cells as model. 5000 cells per well were seeded into a 96-well plate and incubated at 37 ^{o}C in a humidified atmosphere with 5% CO_2. The culture medium was a Dulbecco's modified Eagle's medium (DMEM, Gibco) supplemented with 10% fetal bovine serum (FBS, Hyclone, Logan, UT), streptomycin at 100 μg/mL, penicillin at 100 U mL^{-1}, 4 mM L-glutamine and changed every other day until 80% confluence had been reached. The medium was then replaced with 100 μL of the solution containing SPIO NPs or CS-SPIO hybrid nanospheres at different concentrations. One row of the 96-well plates was used as a control. After incubation for 48 h, 20 μL of MTT solution (5 mg/mL) was added to each well, and the plate was incubated for another 4 h, allowing the viable cells to reduce the yellow MTT to dark-blue formazan crystals. Finally, all medium was removed and the crystals were completely dissolved in 150 μL dimethyl sulphoxide (DMSO). The absorbance of individual wells was measured at 570 nm by an ELISA reader (Huadong, DG-5031, Nanjing). The reported data represented the means of triplicate measurements. The values obtained were expressed as a percentage of the control cells to which no nanoparticles were added.

Cellular uptake of CS-SPIO hybrid nanospheres

The hybrid nanospheres were labeled with FITC. Briefly, 1 mL of anhydrous DMSO containing 1 mg FITC was added into 5 mL CS-SPIO hybrid nanospheres solution, and the mixture was stirred for 24 h at room temperature in the dark. Then, the FITC-labeled CS-SPIO hybrid nanospheres were separated by centrifugation and unreacted FITC was removed. Finally, the obtained FITC-labeled CS-SPIO nanospheres were dispersed in aqueous for in vitro cellular uptake.

The SH-SY5Y cells were seeded at a density of 1×10^5 cells per well in a six-well plate containing a cover glass and allowed to adhere for 24 h in a humidified atmosphere of 5% CO_2 at 37 ^{o}C to achieve a confluence of approximately 80%. The cells were then washed with fresh DMEM medium, and 100 μL of FITC-labeled CS-SPIO hybrid nanospheres was added into the plate. After 4 h of incubation at 37 ^{o}C, the cells were washed three times with PBS at 4 ^{o}C and 37 ^{o}C respectively. 4', 6-diamidino-2-phenylindole (DAPI) was employed to dye the nucleus zone of the cells. The cells were observed by confocal laser scanning microscopy (CLSM; Zeiss LSM 710, Germany) at an excitation wavelength of 488 nm.

Real-time NIRF imaging examination in vivo

NIR-797 isothiocyanate was used to label CS-SPIO hybrid nanospheres. Briefly, 0.5 mg of NIR-797 isothiocyanate in 100 μL of anhydrous DMSO was added to 5 mL of CS-SPIO nanospheres solution, and the solution was stirred 12 h at room temperature in the dark. Unreacted NIR-797 was removed by dialysis against deionized water using dialysis bag (MWCO 14 kDa) for 2 days.

All animal studies were performed in compliance with guidelines set by the Animal Care Committee of Nanjing University. 5×10^5 murine H_{22} cells in 0.1 mL saline were subcutaneously inoculated into the right flank of ICR male mice. The mice were kept 7 days with free access to food and water. The NIR-797 labeled hybrid nanospheres were intravenously administrated into H_{22} tumor-bearing mice after the tumor was established. The time-dependent biodistribution in tumor-bearing mice was imaged using the Maestro EX fluorescence imaging system (CRi, Inc., USA). Light with a central wavelength at 704 nm was selected as the excitation source. Scans were conducted at 1, 2, 4, 8, 12, 24, 36 and 48 h post i.v. administration.

In vivo MR imaging

The H_{22} tumor-bearing ICR mice were administered with SPIO NPs or CS-SPIO hybrid nanospheres by tail vein injection at a dose of 5 mg (Fe)/kg body weight. MR imaging were taken prior to the injection of the magnetic samples and at 8 h post injection, after mice were anesthetized with isoflurane. Three mice were examined for each sample. The in vivo MRI experiments were performed on the 7.0 T Micro-MR scanner (PharmaScan 70/17, Brucker). TR/TE = 2500 ms/33 ms, field of view (FOV) = 4.0 × 4.0 cm, matrix size = 256 × 256. Coronal and transversal cross section images were acquired for each mouse.

Results and discussion

Preparation of CS-SPIO hybrid nanospheres

Superparamagnetic Fe_3O_4 nanoparticles were prepared in tetraethylene glycol (TEG) at elevated temperature without any surfactants. Transmission electron microscopy (TEM) image (Fig. 1a) clearly shows that the obtained Fe_3O_4 nanoparticles are nearly spherical with an average diameter of 8.8 nm (an average of about 200 particles). The high-resolution TEM image in Fig. 1b displays the lattice fringes of as-prepared Fe_3O_4 nanoparticle. The particle appears to be a single crystal and exhibits a 0.25 nm *d*-spacing, corresponding to the distance between 311 planes in spinel-structured Fe_3O_4. Fig. 1c shows X-ray diffraction (XRD) pattern of the sample. It is found that all of the diffraction peaks for the as-synthesized nanoparticles match well with standard Fe_3O_4 powder diffraction data (JCPDS No. 19-0629), demonstrating the formation of Fe_3O_4 nanocrystals. Additionally, the broadening of the diffraction peaks distinctly indicates the nanocrystalline nature of the materials.

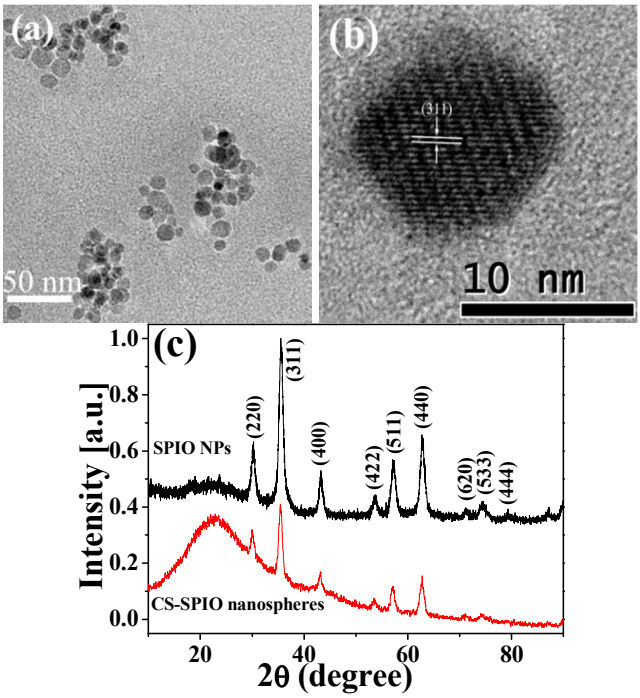

Fig. 1 (a) TEM and (b) high-resolution TEM images of SPIO NPs, (c) XRD patterns of SPIO NPs and CS-SPIO hybrid nanospheres.

The CS-SPIO hybrid nanospheres were prepared through the self-assembly of CS and SPIO driven by the electrostatic interaction between cationic chitosan and anionic EDTA and nonsolvent-aided counterion complexation in the presence of TEG-stabilized Fe_3O_4 NPs. Briefly, purified Fe_3O_4 NPs were dispersed in an aqueous solution containing chitosan and EDTA with the aid of ultrasonication and stirring, then ethanol was added to the aqueous solution as a nonsolvent. The desolvation of chitosan and counterion interactions between CS and EDTA occurred in this process induce the formation of CS-EDTA nanospheres.[44] Meanwhile, Fe_3O_4 NPs were spontaneously incorporated into the CS-EDTA nanospheres by the hydrogen-bonding interaction between EDTA and TEG-stabilized Fe_3O_4 NPs. Subsequently, EDTA component was removed from the hybrid nanospheres after the cross-linking of chitosan moiety by glutaraldehyde and dialysis against water thanks to its small-molecule nature, while the TEG-stabilized Fe_3O_4 nanoparticles were left inside the chitosan spherical network to form CS-SPIO hybrid nanospheres. After non-loaded Fe_3O_4 nanoparticles were removed, the CS-SPIO hybrid nanospheres with cationic chitosan matrix and Fe_3O_4 NPs were obtained. Additionally, the XRD pattern of the CS-SPIO hybrid nanospheres after the EDTA was removed is shown in Fig. 1c. It has been observed that the peak shape and positions of the Fe_3O_4 NPs are invariant before and after encapsulation into the chitosan spheres. Based on the calculation using Scherrer's formula, the SPIO NPs inside the nanospheres retain the same average size as the bare Fe_3O_4 NPs mentioned above. Therefore, the Fe_3O_4 NPs are indeed encapsulated into the chitosan nanospheres and the structure of Fe_3O_4 NPs is unchanged during the self-assembly process.

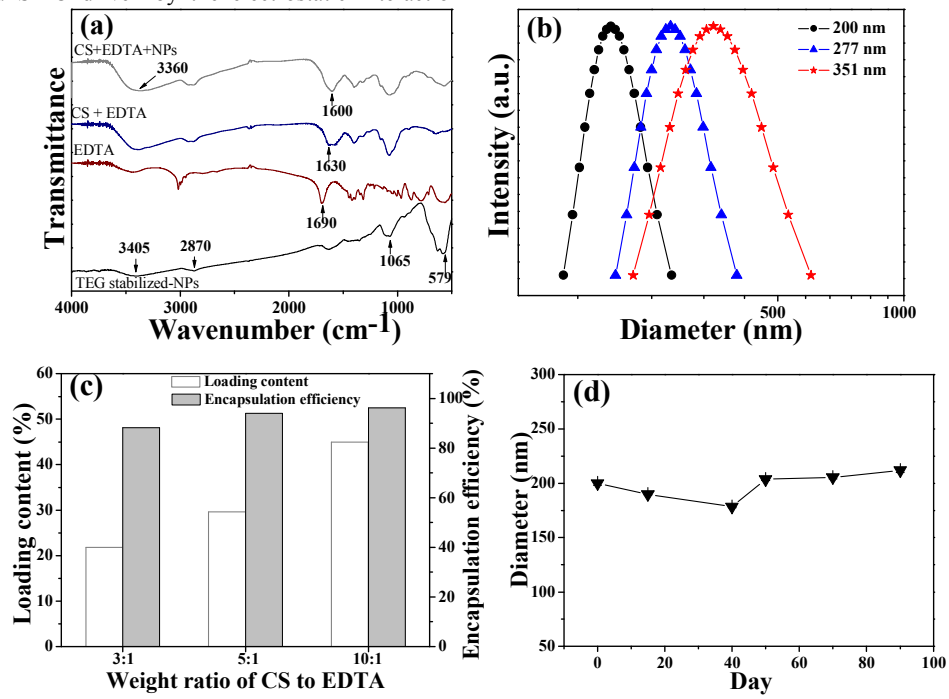

Fig. 2 (a) FT-IR spectra of EDTA, TEG-stabilized Fe_3O_4 NPs, the blend of CS and EDTA, the blend of CS, EDTA and Fe_3O_4 NPs. (b) Size distributions of CS-SPIO hybrid nanospheres prepared from different weight ratios of CS to EDTA (CS : EDTA = 10:1, ●; 5:1, ▲; 3:1, ★). (c) The encapsulation efficiency and loading content of Fe_3O_4 NPs inside the hybrid nanospheres prepared with various weight ratios of CS to EDTA from 3:1 to 10:1. (d) Hydrodynamic diameter of the CS-SPIO-(45) hybrid nanospheres stored in water for three months.

The interaction between TEG-stabilized Fe_3O_4 NPs and EDTA was confirmed by FT-IR spectra as shown in Fig. 2a. A broad band around 3405 cm^{-1} from the O-H stretching vibration of TEG occurs in TEG-stabilized Fe_3O_4 NPs spectrum. A strong metal-O absorption band at around 579 cm^{-1} is also observed, indicating the strong interactions between Fe_3O_4 NPs and TEG molecules. From the FT-IR spectra of EDTA and the blend of CS and EDTA (10:1 w/w), it can be found that the absorption band of the carbonyl group in

EDTA (1690 cm^{-1}) downshifts to a wavenumber of 1630 cm^{-1} in the spectrum of the CS/EDTA blend because of the ionization of the carboxyls in the EDTA molecules. Further the absorption peak of the carbonyl groups of EDTA at 1630 cm^{-1} shifts to 1600 cm^{-1} in the CS/EDTA/Fe_3O_4 NPs blend (CS:EDTA:NP = 10:1:10 w/w/w), indicating the formation of intermolecular hydrogen bonds between TEG-stabilized Fe_3O_4 NPs and EDTA. Thus, it can be deduced that the Fe_3O_4 NPs are mainly located in the interior of the hybrid nanospheres since EDTA moieties are in the interior of the CS-EDTA nanospheres.

To optimize our synthesis parameters, the CS-SPIO hybrid nanospheres were prepared by changing the weight ratio of CS to EDTA, and the size of hybrid nanopsheres formed were monitored by DLS. As shown in Fig. 2b, the hydrodynamic diameter of the CS-SPIO hybrid nanospheres decreases from 351.1 nm to 200 nm when the weight ratio of CS to EDTA changes from 3:1 to 10:1. Meanwhile, as a signal of the amount of Fe_3O_4 NPs in chitosan nanospheres, the loading contents of Fe_3O_4 NPs in the hybrid nanospheres are 22%, 30% and 45%, corresponding to a 3:1, 5:1 and 10:1 for the ratio of CS to EDTA, respectively (Fig. 2c). Herein, these hybrid nanospheres are termed as CS-SPIO-(22), CS-SPIO-(30) and CS-SPIO-(45). It is worth mentioning that the hybrid nanospheres can be fully redispersed by gentle agitation of hand although the large density of the Fe_3O_4 NPs would result in slight sedimentation after 90 days of storage. Moreover, DLS analysis indicates that the particle size almost does not change after redispersion (Fig. 2d).

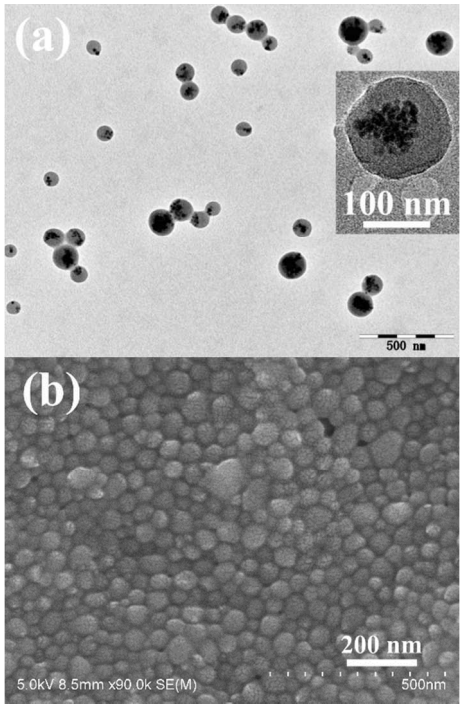

Fig. 3 (a) TEM image and (b) SEM image of CS-SPIO-(45).

Fig. 3 shows the TEM and SEM images of CS-SPIO-(45) hybrid nanospheres. It can be seen that the CS-SPIO hybrid nanospheres have a well-defined spherical morphology and uniform size. Observably, almost all of the Fe_3O_4 NPs are located in the interior of the hybrid nanospheres since the markedly high electron density of Fe_3O_4 NPs enables the direct visualization of Fe_3O_4 NPs. It is important from Fig. 3a that the clustering of the superparamagnetic iron oxide nanoparticles is jamming in the interior of chitosan sphere. These results highlight effectiveness of encapsulated Fe_3O_4 NPs based on the nonsolvent aided counterion complexation method.

Magnetization and T_2 relaxivity of SPIO NPs and hybrid nanospheres

Fig. 4a shows magnetization curves of SPIO nanoparticles and CS-SPIO-(45) hybrid nanospheres at room temperature. Both the SPIO NPs and hybrid nanospheres show typical superparamagnetic behavior, with zero coercivity and remanence. The saturated magnetization (Ms) of the SPIO NPs is about 61.2 emu g^{-1}, while for CS-SPIO-(45) hybrid nanospheres, the Ms is about 58.4 emu g^{-1}. Thus, there is no loss in magnetization per Fe unit before and after encapsulation of the SPIO NPs. Importantly, the crowding and clustering of SPIO NPs in spherical chitosan matrix does not change superparamagnetic character of SPIO NPs.

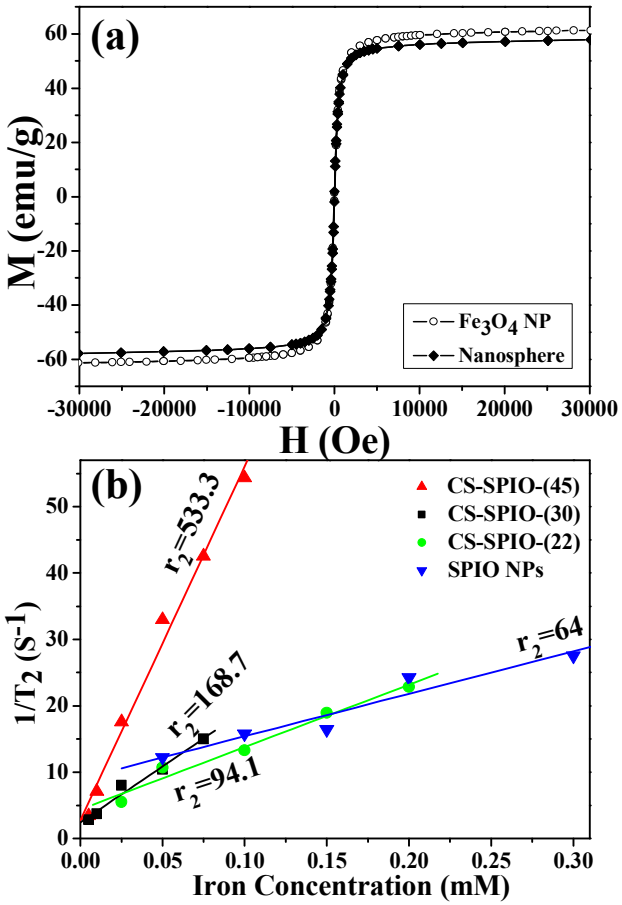

Fig. 4 (a) Magnetization curves at 300 K of SPIO NPs and CS-SPIO-(45) hybrid nanospheres. (b) T_2 relaxation rates ($1/T_2$, s^{-1}) as a function of iron concentration (mM) for SPIO NPs (▼), CS-SPIO-(22) (●), CS-SPIO-(30) (■) and CS-SPIO-(45) (▲), r_2: Fe $mM^{-1}s^{-1}$.

To evaluate the MRI sensitivity of the CS-SPIO hybrid nanospheres as a T_2-contrast agent, the transverse relaxation time (T_2) of the water proton of the aqueous solutions containing SPIO nanoparticles and CS-SPIO hybrid nanospheres was measured, respectively. Generally, the transverse relaxivity r_2 represents the ability of the contrast agent to alter T_2, and is calculated through the

linear least squares fitting of $1/T_2$ (s^{-1}) *versus* the iron concentration (mM Fe).[17] As indicated by the slopes of lines shown in Fig. 4b, encapsulating the Fe_3O_4 NPs into chitosan nanospheres significantly increases r_2 relaxivity of SPIO nanoparticles in comparison to bare ones. The r_2 value of the CS-SPIO hybrid nanospheres increases from 94.1 to 533.3 Fe mM^{-1} s^{-1} when Fe_3O_4 NP loadings increase from 22% to 45%, revealing a loading dependence that a higher payload of Fe_3O_4 nanoparticles inside the chitosan spheres results in a better contrast efficacy. These values, found in Table1, demonstrate that the transversal relaxivity of Fe_3O_4 NPs confined chitosan spheres is all significantly greater than free Fe_3O_4 NPs, with increasing from 47% to 733% for the CS-SPIO hybrid nanospheres, suggesting that increasing the loading of Fe_3O_4 NPs in the hybrid nanospheres will lead to enhanced relaxation rates for the CS-SPIO

Table 1. Preparation parameter and molar transverse relaxivity rate r_2 of hybrid nanospheres

	Feed ratio CS:EDTA (wt/wt)	SPIO loading content (%)	Particle size (nm)	r_2 [Fe $mM^{-1}s^{-1}$]	% increase in r_2*
SPIO NPs	/	/	8.8	64	/
CS-SPIO-(22)	3:1	22	351	94.1	47
CS-SPIO-(30)	5:1	30	277	168.7	164
CS-SPIO-(45)	10:1	45	200	533.3	733

* The increase in the relaxivity of hybrid nanospheres compared to free SPIO nanoparticles

hybrid nanospheres. As mentioned earlier, the loading of Fe_3O_4 NPs in the nanospheres could be tuned by changing feeding ratio in preparation, rendering the hybrid nanospheres highly flexible in terms of r_2 relaxivity control. The dramatic improvement in the relaxivity of the SPIO nanoparticles within hybrid spheres is probably ascribed to following reasons. First, the high payload of SPIO nanoparticles within CS spheres may cause the clustering effect of SPIO nanoparticles in polymer matrix, which enhances the relaxivity of the SPIO nanoparticles, as shown in Fig. 5a. Second, the jamming or crowding of clustered magnetic nanoparticles in the chitosan nanospheres shortens the distance between the clusters of SPIO nanoparticles, leading to a synergistic increase in r_2. Finally,

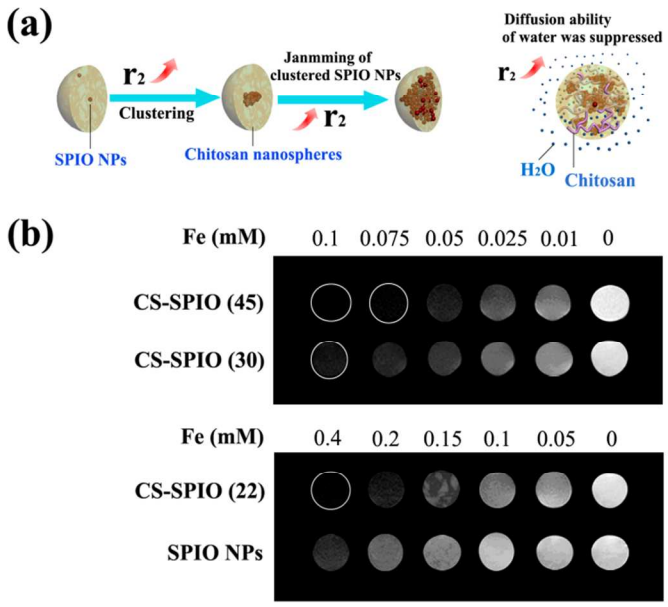

Fig. 5 (a) Schematic illustration of probable mechanism of enhanced transversal relaxivity for the CS-SPIO hybrid nanospheres. (b) T_2-weighted MR images of SPIO NPs and CS-SPIO hybrid nanospheres with different payloads at different Fe concentrations.

the hydrophilic chitosan spherical matrix retards the diffusion of water near the surface of the magnetic nanoparticles and thus prolongs the interaction between the water protons and the magnetic fields near the particle, resulting in the relaxivity enhancement of the SPIO nanoparticles. Thus, the unique architecture of the hybrid nanospheres is a major cause for the enhancement in r_2, which can be used for controlled synthesis of MRI contrast agent with desired r_2 value.

To investigate the effect of CS-SPIO hybrid nanospheres on MRI images, MRI observations were performed in the aqueous samples with different concentrations of contrast agents, and the MRI signal intensities were compared between SPIO nanoparticles and three CS-SPIO hybrid nanospheres. As shown in Fig. 5b, the higher payload of SPIO nanoparticle in hybrid nanospheres, the darker color in the T_2-weighted MR image for a given Fe concentration. This further confirms that jamming SPIO nanoparticles inside confined spherical matrix drastically increases image contrast. It is apparent that the sample with highest payload of SPIO nanoparticles, that is, CS-SPIO-(45) hybrid nanospheres show a darkest color. Thus, CS-SPIO-(45) hybrid nanospheres can serve as highly efficient T_2 contrast agent. Hence, we used the CS-SPIO-(45) hybrid nanospheres in subsequent experiments.

Cytotoxicity and cell internalization of hybrid nanospheres

A standard MTT assay using the HeLa cell line and the SH-SY5Y cell line was performed to assess the in vitro toxicity of the CS-SPIO hybrid nanospheres. The SPIO nanoparticles and CS-SPIO hybrid nanospheres at various concentrations were incubated with HeLa and SH-SY5Y cells for 48 h. As shown in Fig. 6a and 6b, no cytotoxicity is observed for these samples in the tested concentration range, suggesting that the hybrid nanospheres are cytocompatible.

Next the cell internalization and intracellular distribution of the hybrid nanospheres were investigated by CLSM. After FITC-labeled CS-SPIO hybrid nanospheres were incubated with SH-SY5Y cells for 4 h at 37 ^oC and the nuclei were selectively stained blue with DAPI, fluorescent, bright-field, and overlay images of the cells were observed as depicted in Fig. 6c-e. From the fluorescent image, one can see that most of green bright spots occupy the cytoplasm of the cells and the fluorescent signals are not evenly distributed in cells. These results together along the green punctate fluorescence patterns exhibited in the cells imply that the hybrid nanospheres can be efficiently internalized following an endocytosis uptake mechanism. Thus, CS-SPIO hybrid nanospheres can effectively internalized by cancer cells.

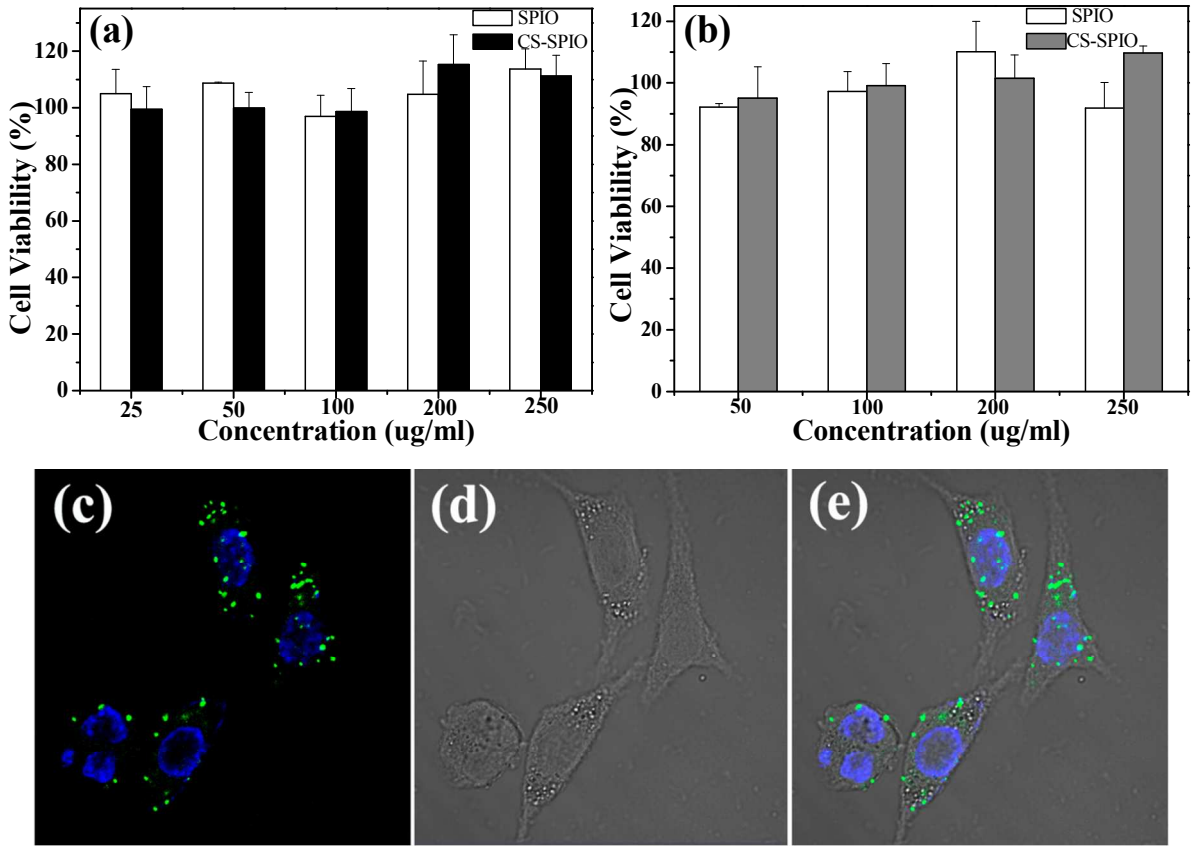

Fig. 6 Viability of SH-SY5Y cells (a) and HeLa cells (b) incubated with SPIO NPs and CS-SPIO hybrid nanospheres. The bare SPIO NPs concentration was set at the same level as the embedded SPIO NPs in the hybrid nanospheres. The results represent the mean ± SD (n = 3). (c) Confocal fluorescent, (d) bright-field, and (e) overlay images of SH-SY5Y cells incubated with FITC-labeled CS-SPIO hybrid nanospheres (green) for 4 h, at 37 ºC. The cell nuclei were stained by DAPI (blue).

In vivo MRI and fate of hybrid nanospheres

To further examine the imaging ability of hybrid nanospheres, we investigated the potential of the CS-SPIO hybrid nanospheres for *in vivo* tumor MR imaging. To evaluate the in vivo performance of the hybrid nanospheres more clearly, the SPIO nanoparticles was examined in parallel as references. The CS-SPIO hybrid nanospheres and SPIO nanoprticles were injected via a tail vein into two groups of H_{22} tumor-bearing mice, respectively. The dose of Fe used in this experiment is comparatively lower than used in recently report.[6,15-16] T_2-weighted MR images acquired in H_{22} tumor-bearing mice before and after injection are shown in Fig. 7. As can be seen in Fig. 7a, the region of interest (ROI) in the tumor, marked by a dotted circle, exhibits noticeable hypiontensity at 8 h after injection of the CS-SPIO hybrid nanospheres, revealing the hybrid nanospheres has selectively accumulated in the tumor due to enhanced permeability and retention effect (EPR). Herein, inhomogenous darkening effect in tumors can be attributed to inhomogeneous distribution of neovasculature and poor permeability of the hybrid nanospheres within the tumor. In contrast, no significant change in tumor tissue is found after injection of the SPIO nanoparticles under the same injected dose (Fig. 7b), whereas the MRI signal in the liver drops dramatically. This indicates that the separate Fe_3O_4 NPs have poor function of T_2-weighted contrast agents for tumor imaging at the low dose used in the test. Therefore, it is reasonable to say that the CS-SPIO hybrid nanospheres have an excellent tumor imaging ability in tumor-bearing mice. It is worth pointing that the mice recovered from anesthesia spontaneously after the experiment and lived normally for weeks. This demonstrates that the CS-SPIO hybrid nanospheres are not acute toxic to the experimental animals. Thus, the CS-SPIO hybrid nanospheres can be used as MRI T_2 negative contrast agent and have great potential for noninvasive tumor diagnosis.

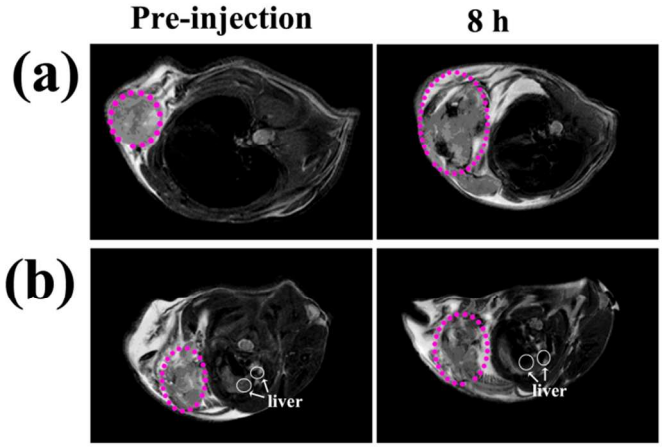

Fig. 7 T_2-weighted MR images of H22 tumor-bearing mice acquired before and 8 h after the i.v. injection of CS-SPIO hybrid nanospheres (a), and SPIO nanoparticles (b).

To further investigate the fate of the hybrid nanospheres in a living system, a real time NIR fluorescence imaging technique was utilized. The CS-SPIO hybrid nanospheres labeled with a NIR fluorescence dye, NIR-797, were injected into subcutaneous hepatic H_{22} tumor-bearing mice via the vein. Fig. 8 depicts the *in vivo* fluorescence distribution of NIR-797 labeled hybrid nanospheres at different time after injection. The different fluorescence intensities are represented by different colors as shown in color histogram. It can be seen that the strong fluorescence signals are observed in the liver and intestine in the initial 4 h post-injection, suggesting that partial CS-SPIO hybrid nanospheres accumulate in these organs and are rapidly captured by the reticuloendothelial system (RES). At 8 h post-injection, the fluorescence signal of the hybrid nanospheres appears in tumor site and becomes stronger and stronger as time escapes. Compared to the tumor, the fluorescence intensity in liver tissue decreases gradually from 36 h post-injection. These results demonstrate that the CS-SPIO hybrid nanospheres have a significant EPR effect driven passive targeting ability toward tumor accumulation. Take together, the *in vivo* MRI and the *in vivo* NIR fluorescence imaging results indicate that the hybrid nanospheres successfully accumulated in the tumor tissue, providing an efficient candidate in vivo MRI contrast agent for cancer diagnosis.

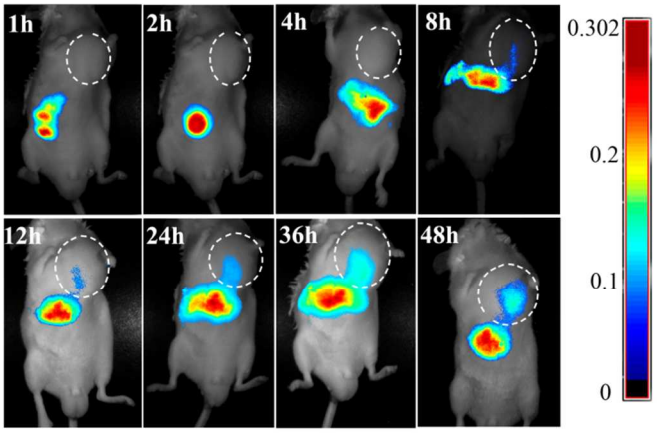

Fig. 8 The NIRF images of tumor-bearing mice following i.v. injection of NIR-797 labeled CS-SPIO hybrid nanospheres. Tumor areas were surrounded with dashed circle.

Conclusions

In summary, the CS-SPIO hybrid nanospheres using as MRI contrast agents were successfully prepared. The architecture of SPIO nanoparticle clusters in a jamming fashion inside hydrophilic chitosan spherical matrix significantly increases the r_2 relaxivity of the CS-SPIO nanospheres, endowing a higher value of relaxivities for the hybrid nanospheres (up to 533.3 Fe mM^{-1} s^{-1}) than that of separate SPIO NPs (64 Fe mM^{-1} s^{-1}). The desired size of hybrid spheres and payload of SPIO nanoparticles within the spheres are achieved by varying the ratio of CS to EDTA, leading to controllable r_2 relaxivity for CS-SPIO hybrid nanospheres. In addition, the obtained hybrid nanospheres show a good colloidal stability and cytocompatibility. Meanwhile, in vitro fluorescence imaging observations reveal that the hybrid nanospheres can be taken-up by cancer cells, making them suitable for cancer-cell imaging. In vivo MR imaging and NIR fluorescence imaging in tumor-bearing mice show that the CS-SPIO hybrid nanospheres can be enriched remarkably in the tumor due to EPR effect, leading to a high MR signal contrast in the tumor at a relatively low dose of Fe. The demonstrated high MRI sensitivity, tunable r_2 relaxivity, passive targeting function, abundant functional groups on the surface of the CS-SPIO hybrid nanospheres support the use of these nanospheres as effective T_2 MRI contrast agents for accurate cancer diagnosis.

Acknowledgements

This study was supported by the Natural Science Foundation of China (51303003, 21474045, 51273090 and 51303002), the Natural Science Foundation of Anhui Province (1408085QE76), Program for Changjiang Scholars and Innovative Research Team in University, and Specialized Research Fund for the Doctoral Program of Higher Education

[a] *School of Biology and Chemical Engineering, Anhui Polytechnic University, Wuhu 241000, P. R. China*
[b] *Department of Polymer Science & Engineering, College of Chemistry & Chemical Engineering, Nanjing University, Nanjing 210093, P. R. China*
Fax: 86 25 83597138; E-mail: jiangx@nju.edu.cn.

Notes and references

1 J. Shen, C. Zhou, X. Zhong, R. Guo, J. F. Griffith, L. Cheng, X. Duan and B. Liang, *Radiology*, 2010, **254**, 729.
2 R. Weissleder, K. Kelly, E. Y. Sun, T. Shtatland and L. Josephson, *Nat. Biotechnol.*, 2005, **23**, 1418.
3 S. Laurent, D. Forge, M. Port, A. Roch, C. Robic, L. V. Elst and R. N. Muller, *Chem. Rev.*, 2008, **108**, 2064.
4 G. Wang, S. Inturi, N. J. Serkova, S. Merkulov, K. McCrae, S. E. Russek, N. K. Banda and D. Simberg, *ACS Nano*, 2014, **8**, 12437.
5 D. Cheng, G. Hong, W. Wang, R. Yuan, H. Ai, J. Shen, B. Liang, J. Gao and X. Shuai, *J. Mater. Chem.*, 2011, **21**, 4796.
6 S. Aryal, J. Key, C. Stigliano, J. S. Ananta, M. Zhong and P. Decuzzi, *Biomaterials*, 2013, **34**, 7725.
7 G. Liu, Z. Wang, J. Lu, C. Xia, F. Cao, Q. Gong, B. Song, X. Zhao, X. Shuai, X. Chen, H. Ai and Z. Gu, *Biomaterials*, 2011, **32**, 528.
8 R. D. Corato, F. Gazeau, C. L.Visage, D. Fayol, P. Levitz, F. Lux, D. Letourneur, N. Luciani, O. Tillement and C. Wilhelm, *ACS Nano*, 2013, **7**, 7500.
9 S. Naqvi, M. Samim, M. Abdin, F. J. Ahmed, A. Matitra, C. Prashant and A. K. Dinda, *Int. J. Nanomed.*, 2010, **5**, 983.
10 S. J. H. Soenen, U. Himmelreich, N. Nuytten and M. D. Cuyper, *Biomaterials*, 2011, **32**, 195.
11 B. Wang, W. Feng, M. Zhu, Y. Wang, M. Wang, Y. Gu, H. Ouyang, Y. Zhao, Z. Chai and H. Wang, *J. Nanopart. Res.*, 2008, **11**, 41.
12 E. Pöselt, H. Kloust, U. Tromsdorf, M. Janschel, C. Hahn, C. Maβlo and H. Weller, *ACS Nano*, 2012, **6**, 1619.
13 D. Liu, W. Wu, J. Ling, S. Wen, N. Gu and X. Zhang, *Adv. Funct. Mater.*, 2011, **21**, 1498.

14 A. Ruiz, G. Salas, M. Calero, Y. Hernández, A. Villanueva, F. Herranz, S. Veintemillas-Verdaguer, E. Martínez, D. F. Barber and M. P. Morales, *Acta Biomater.*, 2013, **9**, 6421.
15 A. P. Khandhar, R. M. Ferguson, H. Arami and K. M. Krishnan, *Biomaterials*, 2013, **34**, 3837.
16 H. Yang, C. W. Park, P. K. Bae, T. Ahn, B. Seo, B. H. Chung and J. Kim, *J. Mater. Chem. B*, 2013, **1**, 3035.
17 Y. Lin, W. Yao, Y. Cheng, H. Qian, X. Wang, Y. Ding, W. Wu and X. Jiang, *J. Mater. Chem.*, 2012, **22**, 5684.
18 M. H. Pablico-Lansigan, W. J. Hickling, E. A. Japp, O. C. Rodriguez, A. Ghosh, C. Albanese, M. Nishida, E. V. Keuren, S. Fricke, N. Dollahon and S. L. Stoll, *ACS Nano*, 2013, **7**, 9040.
19 Y. Jun, J. Lee and J. Cheon, *Angew. Chem. Int. Ed.*, 2008, **47**, 5122.
20 A. Saraswathy, S. S. Nazeer, N. Nimi, S. Arumugam, S. J. Shenoy and R. S. Jayasree, *Carbohydr. Polym.*, 2014, **101**, 760.
21 A. Saraswathy, S. S. Nazeer, M. Jeevan, N. Nimi, S. Arumugam, V. S. Harikrishnan and R. S. Jayasree, *Colloids Surf. B: Biointerfaces*, 2014, **117**, 216.
22 G. Huang, H. Li, J. Chen, Z. Zhao, L. Yang, X. Chi, Z. Chen, X. Wang and J. Gao, *Nanoscale*, 2014, **6**, 10404.
23 J. Jang, H. Nah, J. Lee, S. H. Moon, M. G. Kim and J. Cheon, *Angew. Chem. Int. Ed.*, 2009, **48**, 1234.
24 A. E. Beeran, S. S. Nazeer, F. B. Fernandez, K. S. Muvvala, W. Wunderlich, A. John, R. S. Jayasree and P. R. H. Varma, *Phys. Chem. Chem. Phys.*, 2015, **17**, 4609.
25 C. Paquet, H. W. Haan, D. M. Leek, H. Lin, B. Xiang, G. Tian, A. Kell and B. Simard, *ACS Nano*, 2011, **5**, 3104.
26 H. W. Haan and C. Paquet, *Magn. Reson. Med.*, 2011, **66**, 1759.
27 Y. Chen, J. Nan, Y. Lu, C. Wang, F. Chu and Z. Gu, *J. Biomed. Nanotechnol.*, 2015, **11**, 771.
28 E. Choo, X. Tang, Y. Sheng, B. Shuter and J. Xue, *J. Mater. Chem.*, 2011, **21**, 2310.
29 L. Josephson, J. M. Perez and R. Weissleder, *Angew. Chem. Int. Ed.*, 2001, **40**, 3204.
30 Q. L. Vuong, P. Gillis and Y. Gossuin, *J. Magn. Reson.*, 2011, **212**, 139.
31 R. J. Hickey, X. Meng, P. Zhang and S. Park, *ACS Nano*, 2013, **7**, 5824.
32 F. Ye, A. Barrefelt, H. Asem, M. Abedi-Valugerdi, I. EI-Serafi, M. Saghafian, K. Abu-Salah and M. Hassan, *Biomaterials*, 2014, **35**, 3885.
33 Q. L. Vuong, J. Berret, J. Fresnais, Y. Gossuin and O. Sandre, *Adv. Healthcare Mater.*, 2012, **1**, 502.
34 Y. Hu, L. Meng, L. Niu and Q. Lu, *Langmuir*, 2013, **29**, 9156.
35 Y. Wang, F. Xu, C. Zhang, D. Lei, Y. Tang, H. Xu, Z. Zhang, H. Lu, X. Du, G. Yang, *Nanomed-Nanotechnol.*, 2011, **7**, 1009.
36 C. Zhang, X. Xie, S. Liang, M. Li, Y. Liu, H. Gu, *Nanomed-Nanotechnol.*, 2012, **8**, 996.
37 U. I. Tromsdorf, N. C. Bigall, M. G. Kaul, O. T. Bruns, M. S. Nikolic, B. Mollwitz, R. A. Sperling, R. Reimer, H. Hohenberg, W. J. Parak, S. Förster, U. Beisiegel, G. Adam, H. Weller, *Nano Lett.*, 2007, **7**, 2422.
38 J. Wang, Z. Zhang, X. Wang, W. Wu and X. Jiang, *J. Control. Release*, 2013, **168**, 1.
39 R. Chen, X. Wang, X. Yao, X. Zheng, J. Wang and X. Jiang, *Biomaterials*, 2013, **34**, 8314.
40 L. Upadhyaya, J. Singh, V. Agarwal and R. P. Tewari, *J. Control. Release*, 2014, **186**, 54.
41 J. H. Ryu, Y. Lee, W. H. Kong, T. G. Kim, T. G. Park and H. Lee, *Biomacromolecules*, 2011, **12**, 2653.
42 S. A. Agnihotri, N. N. Mallikarjuna and T. M. Aminabhavi, *J. Control. Release*, 2004, **100**, 5.
43 J. Wan, W. Cai, X. Meng and E. Liu, *Chem. Commun.*, 2007, **47**, 5004.
44 R. Guo, L. Zhang, Z. Zhu and X. Jiang, *Langmuir*, 2008, **24**, 3459.

Table of Contents

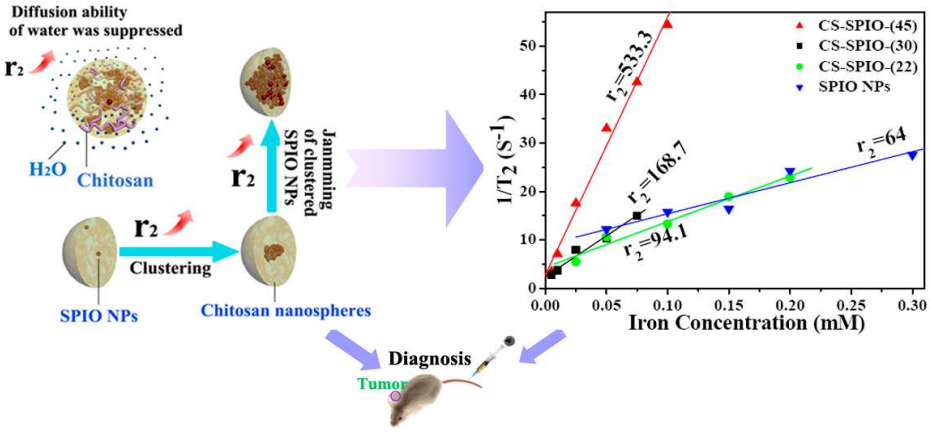

Highlighting sentence: An ultra-high relaxivity of MRI contrast agent were fabricated controllable by clustering iron oxide nanoparticles confined in hydrophilic polymer.